Journal of Robotics and Control (JRC)
Volume 3, Issue 5, September 2022
ISSN: 2715-5072, DOI: 10.18196/jrc.v3i5.1604

Optimizing the Dynamic Performance of a Wind Driven Standalone DFIG Using an Advanced Control Algorithm

Mahmoud K. Abdelhamid [1], Mahmoud A. Mossa [2*], Ahmed A. Hassan [3]
[1,2,3]Electrical Engineering Department, Faculty of Engineering, Minia University, Minia 61111, Egypt
Email: [1] mahmoud_khalifa@mu.edu.eg, [2] mahmoud_a_mossa@mu.edu.eg, [3] ahmed.hasan@mu.edu.eg
*Corresponding Author

***Abstract*—The article seeks to improve the dynamic performance of a standalone doubly fed induction generator (DFIG) which driven by a wind turbine, with the help of an effective control approach. The superiority of the designed predictive controller can be confirmed through evaluating the performance of the DFIG under other control algorithm, which is the model predictive direct torque control (MPDTC), model predictive current control (MPCC) as classic types of control. Firstly, the operating principles of the two controllers are described in details. After that, a comprehensive comparison is performed among the dynamic performances of the designed MPDTC, MPCC techniques and the predictive control strategy, so we can easily present the merits and deficiencies of each control scheme to be able to easily select the most appropriate algorithm to be utilized with the DFIG. The comparison is carried out in terms of system simplicity, dynamic response, ripples' content, number of performed commutations and total harmonic distortion (THD). The results of the comparison prove the effectiveness and validation of our proposed predictive controller; as it achieves the system simplicity, its dynamic response is faster than that of MPDTC and MPCC, it presents a lower content of ripples compared to MPDTC and MPCC. Moreover, it can minimize the computational burden, remarkably. Furthermore, the numerical results are showing a marked reduction in the THD with a percentage of 2.23 % compared to MPDTC and 1.8 % compared to MPCC. For these reasons, it can be said that the formulated controller is the most convenient to be used with the DFIG to achieve the best dynamic performance.**

Keywords—DFIG; Standalone; Wind; Predictive Control; Dynamic response; Ripples' content; Computational burden; THD.

I. INTRODUCTION

Energy in general, and electrical energy in particular, is the mainstay for achieving comprehensive and continuous development, it is the heart of all the changes facing society, whether they are social, economic or other. Therefore, generating and providing electricity at an appropriate cost has become indispensable, which prompted researchers to try to find the optimal way to generate electricity. The electricity generation can be performed through either conventional energy resources or renewable energy resources. As the non-renewable energy sources began to decrease day by day remarkably, the current trend became towards the renewable energy sources, such as solar, wind, wave and geothermal energies [1-4].There are different types of electric generators that are utilized to generate electricity through renewable energy resources, like synchronous generator (SG), self-excited induction generator (SEIG), and doubly fed induction generator (DFIG) [5-10]. The DFIG has been frequently utilized with wind turbines over recent years and is still in use, this overall system is called as wind energy conversion system (WECS). The reason to use the DFIG with the WECS is its many advantages, as it proved its worth to operate during the changes of the wind speed while maintaining a constant load voltage and constant frequency. Moreover, its control is flexible, as it can be performed either in the stator or rotor sides [11-19].

There are many control techniques used with the DFIG to try to improve its dynamic performance. In [20, 21], the adopted strategy is the vector orientation control (VOC), this method of control succeeded in improving the torque response and minimizing the ripples' content; unfortunately, it needs to coordinate transformations and depends in its operation on the generator parameters. Furthermore, it uses proportional–integral (PI) regulators, which caused a delay in the system response and some complications.

Another topology of control which used with the DFIG is the direct torque control (DTC) technique, which adopted in [22-26], this methodology excluded the PI regulators which used by VOC approach and replaced them with hysteresis comparators, which leads to avoiding the complications caused due to using PI controllers, and also getting a faster dynamic response compared to VOC technique. Moreover, it doesn't need to coordinate transformations, as the control is performed in the alpha-beta $(\alpha - \beta)$ frame; but on the other hand, it has more ripples than VOC approach.

Eventually, the researchers have tried to find a new method that can overcome the problems of classic control systems, so the predictive control (PC) strategy came to light, as it has managed to obviate the shortages which face the VOC and DTC techniques [27-32].

The model predictive direct torque control (MPDTC) strategy depends in its operation on minimizing the difference among the reference and predicted components of the torque; and rotor flux, the main goal of this approach is to overcome the defects of DTC technique, the most important of which is the ripples issue, which was overcome by this method of control. Furthermore, it improved the torque

response and made it faster. The MPDTC scheme is still suffering from some defects, its cost function needs to a weighting factor (ω_f) to achieve the equilibrium between the values of the torque and rotor flux errors. Moreover, the computation time is considered as a principal problem which faces this technique; also, the variables of the cost function need for estimation, so this methodology depends on the machine parameters [33, 34].

Another topology of the PC is the model predictive current control (MPCC), which eliminates the using of the weighting factor which is adopted by the MPDTC, also, it minimized the ripples. On the other hand, its dynamic response is slower than that of MPDTC and it still suffers from high calculation time. Furthermore, its cost function contains variables which are calculated utilizing the model parameters, which can be easily affected by the operating conditions [35, 36].

The researchers started to search for a control algorithm, which can beat the most of defects which face other previous classic controllers. Following these research attitudes, we present in the current article a newly efficient and advanced control algorithm, which adopt a very simple cost function with analogous terms, so that, it doesn't require a weighting scale as in case of MPDTC and MPCC. The terms of the cost function are the differences between the reference and predicted actual values of the d-q components of the rotor voltage, a detailed design for the derivation of the d-q components of the voltage references is introduced. Moreover, this methodology of control has a high robustness against the system uncertainties, as its cost function doesn't contain any estimated variables.

Moreover, a detailed comparison between the dynamic performances achieved by the adopted controllers must be performed to outline the features and deficiencies of each topology and easily identify the most efficient algorithm to be used with the DFIG. The comparison is carried out between the designed controller and MPDTC scheme in terms of dynamic response, content of ripples and computational burden.

The article contributions can be summarized as follows:

- The paper introduces a design for an advanced control algorithm which achieved the control targets and improved the DFIG's performance, remarkably.
- The paper performs a detailed dynamic performance analysis for the DFIG using the designed PVC scheme and also for the MPDTC and MPCC techniques under different operating wind speeds.
- The operating principles of the three adopted controllers are introduced in details.
- A detailed comparison of the dynamic performance of the DFIG under the used controllers is performed to outline the effectiveness and robustness of our proposed predictive control algorithm.
- The results of the comparison confirm the validation and superiority of our formulated controller, which was evident in terms of lower dynamic response time, reduced content of ripples, minimized computational time and THD.
- The formulated control algorithm can be utilized with other generator configurations, taking into account differences in structure and principle of operation.

The present paper is arranged as follows: At first, the model of the wind turbine is introduced, then, the mathematical model of the DFIG is described in details, after that, the construction and operating principle of the MPDTC, MPCC and the proposed controllers are introduced. Subsequently, the results of the performed tests are outlined and analyzed, eventually, the conclusions are introduced.

II. WIND ENERGY CONVERSION SYSTEM

A. Modeling of the Wind Turbine

The wind turbine model is shown in Fig. 1, in which the turbine drives a DFIG which supplies an isolated load, the overall system is defined as wind energy conversion system (WECS). The speed of the DFIG is denoted by (ω_g), meanwhile the turbine speed is expressed by (ω_t). As known, we can manage the speed of the turbine via two methods: the first one is through managing the blade pitch angle (β) or by controlling the generator torque (T_g). There's an important ratio which used for evaluating the speed of the turbine, it's called as tip speed ratio (TSR), and can be expressed by:

$$\lambda = \frac{\omega_t R}{V_\omega} \tag{1}$$

where R refers to the radius of the blade.

The power of the wind (P_ω) can be represented by:

$$P_\omega = 0.5\rho A V_\omega^3 \tag{2}$$

Where ρ and A refer to the air density and swept area, respectively.

The power of the turbine (P_t) can be expressed by:

$$P_t = C_p P_\omega = 0.5\rho A C_p V_\omega^3 \tag{3}$$

The power coefficient (C_p) can be represented in terms of (TSR), and (β) as following:

$$C_p = [0.5 - 0.00167(\beta - 2)]\, sin\left[\frac{\pi(\lambda + 0.1)}{10 - 0.3(\beta - 2)}\right] - 0.00184(\lambda - 3)(\beta - 2) \tag{4}$$

The turbine torque (T_t) can be calculated as following:

$$T_t = \frac{P_t}{\omega_t} = \frac{0.5\rho A C_p V_\omega^3}{\omega_t} \tag{5}$$

There's an urgent need for using a gearbox ratio(G) to achieve the equilibrium among the turbine's shaft and the generator's shaft, so the speed of the generator's shaft is related to the turbine speed by the following relationship:

$$\omega_g = G\omega_t \tag{6}$$

The torque of the DFIG's shaft can be represented by:

$$T_g = \frac{T_t}{G} \tag{7}$$

We can represent the mechanical shaft by utilizing a two-mass model as following:

$$T_t - GT_g - FG\omega_t = \left(\frac{J_t}{G} + GJ_g\right)\frac{d\omega_t}{dt} \quad (8)$$

where F is the friction constant, while J_t and J_g refer to the inertia of the turbine and generator, respectively.

The turbine must be managed to operate at an optimal value of TSR (λ_{opt}), to be able to extract the maximum available power; the reference values of turbine and generator speeds which can handle this condition can be represented by:

$$\omega_t^* = \frac{\lambda_{opt} V_\omega}{R} \quad (9)$$

$$\omega_g^* = G\omega_t^* \quad (10)$$

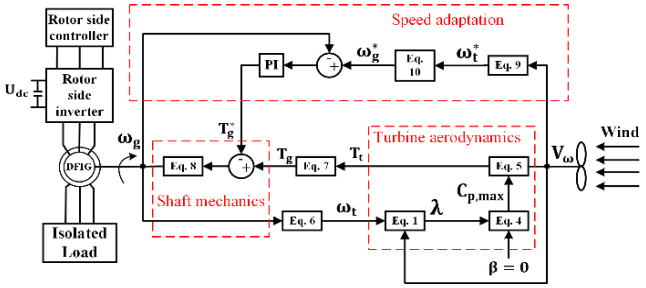

Fig. 1. Model of wind turbine

B. Modeling of the DFIG

The equivalent circuit of the DFIG in the synchronous frame, is shown in Fig. 2. The stator voltage vector $(\bar{u}_{s,k}^{sv})$ was selected to be aligned with the direct axis of the synchronous frame, so the parameters are expressed in a frame which revolves with a speed equal to that of the stator voltage vector $(\omega_{\bar{u}_s})$.

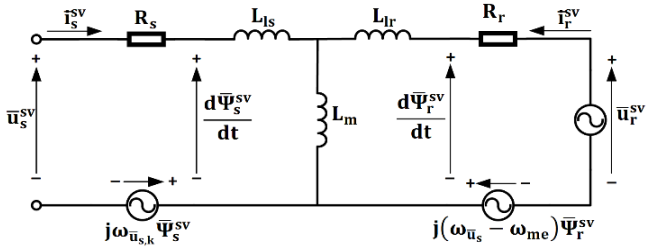

Fig. 2. Equivalent circuit of DFIG

From Fig. 2, and utilizing a sampling time (T_s), we can represent the balance equations of the stator and rotor at instant (KT_s) as following:

$$u_{ds,k}^{sv} = R_s i_{ds,k}^{sv} + \frac{d\Psi_{ds,k}^{sv}}{dt} - \omega_{\bar{u}_{s,k}} \Psi_{qs,k}^{sv} \quad (11)$$

$$u_{qs,k}^{sv} = R_s i_{qs,k}^{sv} + \frac{d\Psi_{qs,k}^{sv}}{dt} + \omega_{\bar{u}_{s,k}} \Psi_{ds,k}^{sv} \quad (12)$$

$$u_{dr,k}^{sv} = R_r i_{dr,k}^{sv} + \frac{d\Psi_{dr,k}^{sv}}{dt} - \overbrace{\left(\omega_{\bar{u}_{s,k}} - \omega_{me,k}\right)}^{\omega_{slip,k}} \Psi_{qr,k}^{sv} \quad (13)$$

$$u_{qr,k}^{sv} = R_r i_{qr,k}^{sv} + \frac{d\Psi_{qr,k}^{sv}}{dt} + \omega_{slip,k} \Psi_{dr,k}^{sv} \quad (14)$$

Where $u_{ds,k}^{sv}$ and $u_{qs,k}^{sv}$ are the d-q components of the stator voltage; $u_{dr,k}^{sv}$ *and* $u_{qr,k}^{sv}$ refer to the d-q components of the rotor voltage; R_s and R_r are the stator and rotor resistances, respectively; $i_{ds,k}^{sv}$ and $i_{qs,k}^{sv}$ denote the d-q components of the stator current; $i_{dr,k}^{sv}$ and $i_{qr,k}^{sv}$ are the d-q components of the rotor current; $\Psi_{ds,k}^{sv}$ and $\Psi_{qs,k}^{sv}$ refer to the d-q components of the stator flux; $\Psi_{dr,k}^{sv}$ and $\Psi_{qr,k}^{sv}$ are the d-q components of the rotor flux; ω_{me} refers to the angular mechanical speed of the rotor; the superscript $'sv'$ clarifies that all parameters are represented in the synchronous frame which revolves with a speed of $\omega_{\bar{u}_s}$.

The d-q components of the stator and rotor flux can be evaluated as follows:

$$\Psi_{ds,k}^{sv} = L_s i_{ds,k}^{sv} + L_m i_{dr,k}^{sv} \quad (15)$$

$$\Psi_{qs,k}^{sv} = L_s i_{qs,k}^{sv} + L_m i_{qr,k}^{sv} \quad (16)$$

$$\Psi_{dr,k}^{sv} = L_r i_{dr,k}^{sv} + L_m i_{ds,k}^{sv} \quad (17)$$

$$\Psi_{qr,k}^{sv} = L_r i_{qr,k}^{sv} + L_m i_{qs,k}^{sv} \quad (18)$$

Where $L_m$denote the mutual inductance; L_s and L_r refer to the stator and rotor inductances, which can be represented as:

$$L_s = L_{ls} + L_m \quad (19)$$

$$L_r = L_{lr} + L_m \quad (20)$$

Where L_{ls} and L_{lr} denote the stator and rotor leakage inductances, respectively.

As mentioned in [37], the d-q derivative components of the rotor current can be found as follows:

$$\frac{di_{dr,k}^{sv}}{dt} = \frac{L_m^2 + L_r L_t}{L_r^2 L_t}\left[u_{dr,k}^{sv} - R_r i_{dr,k}^{sv} + \frac{L_r}{L_m}\omega_{slip,k}\left(\Psi_{qs,k}^{sv} - L_t i_{qs,k}^{sv}\right)\right] - \frac{L_m}{L_r L_t}\left(u_{ds,k}^{sv} - R_s i_{ds,k}^{sv} + \omega_{\bar{u}_{s,k}} \Psi_{qs,k}^{sv}\right) \quad (21)$$

$$\frac{di_{qr,k}^{sv}}{dt} = \frac{L_m^2 + L_r L_t}{L_r^2 L_t}\left[u_{qr,k}^{sv} - R_r i_{qr,k}^{sv} - \frac{L_r}{L_m}\omega_{slip,k}\left(\Psi_{ds,k}^{sv} - L_t i_{ds,k}^{sv}\right)\right] - \frac{L_m}{L_r L_t}\left(u_{qs,k}^{sv} - R_s i_{qs,k}^{sv} - \omega_{\bar{u}_{s,k}} \Psi_{ds,k}^{sv}\right) \quad (22)$$

Where $\left(L_t = \sigma L_s = L_s - \frac{L_m^2}{L_r}\right)$, and refers to the stator transient inductance; $\left(\sigma = 1 - \frac{L_m^2}{L_s L_r}\right)$ refers to the leakage factor.

The mechanical formulation which describes the dynamics of the DFIG can be formulated as:

$$\frac{d\omega_{me,k}}{dt} = \frac{p}{J}\left(T_{me,k} - T_{em,k}\right) \quad (23)$$

Where T_{me} refers to the applied mechanical torque; $T_{em,k}$ denote the electromagnetic torque which developed by the DFIG and can be defined by:

$$T_{em,k} = 1.5pL_m\left(i_{dr,k}^{sv} i_{qs,k}^{sv} - i_{qr,k}^{sv} i_{ds,k}^{sv}\right) \quad (24)$$

Where p and J refer to the number of pole pairs and moment of inertia of the DFIG, respectively.

III. CONTROL TECHNIQUES OF DFIG

A. MPDTC Technique

The MPDTC algorithm is described in details in [12, 19]. The cost function which was utilized in this strategy can be defined by:

$$\Gamma^i = \left|T_{em,k+1}^* - T_{em,k+1}\right|^i + \omega_f \left|\left|\bar{\Psi}_{r,k+1}^*\right| - \left|\bar{\Psi}_{r,k+1}^{sv}\right|\right|^i \quad (25)$$

where the superscript $'i'$ represents the sectors (0, …., 7).

As it's obvious in (25), the MPDTC depends in its operation on minimizing the error among the reference and predicted components of the torque $\left(T_{em,k+1}^* \text{ and } T_{em,k+1}\right)$, and between the reference and predicted components of the rotor flux $\left(\left|\bar{\Psi}_{r,k+1}^*\right| \text{ and } \left|\bar{\Psi}_{r,k+1}^{sv}\right|\right)$.

As mentioned previously, the stator voltage vector $\left(\bar{u}_{s,k+1}^{sv}\right)$ is oriented with the d-axis of the synchronous frame, i.e., the stator voltage-oriented control (SVOC) is adopted here. The following relations can be deduced under SVOC:

$$u_{ds,k+1}^{sv} = \left|\bar{u}_{s,k+1}^{sv}\right| \quad \text{and} \quad u_{qs,k+1}^{sv} = 0.0 \quad (26)$$

$$\Psi_{ds,k+1}^{sv} \approx 0.0 \quad \text{and} \quad \Psi_{qs,k+1}^{sv} \approx -\frac{u_{ds,k+1}^{sv}}{\omega_{\bar{u}_{s,k+1}}} \quad (27)$$

$$i_{ds,k+1}^{sv} = -\left(\frac{L_m}{L_s}\right) i_{dr,k+1}^{sv} \quad (28)$$

$$i_{qs,k+1}^{sv} = \frac{\Psi_{qs,k+1}^{sv}}{L_s} - \left(\frac{L_m}{L_s}\right) i_{qr,k+1}^{sv} = -\left(\frac{L_m}{L_s}\right) i_{qr,k+1}^{sv} - \frac{u_{ds,k+1}^{sv}}{\omega_{\bar{u}_{s,k+1}} L_s} \quad (29)$$

The schematic diagram of the MPDTC is shown in Fig. 3. As noted in the scheme, the reference rotor current component $\left(i_{dr,k+1}^*\right)$ is obtained utilizing the error value of the load active power with the help of PI power regulator, meanwhile, the reference rotor current component $\left(i_{qr,k+1}^*\right)$ is evaluated using the error value of the load voltage magnitude with the aid of PI voltage regulator; to obtain the required load power and at the same time keep the load voltage constant all time which is considered as a basic requirement for standalone systems. The reference stator current component $\left(i_{ds,k+1}^* \text{ and } i_{qr,k+1}^*\right)$ can be easily calculated using (28) and (29), respectively.

It is worth to be mentioned that, the standalone system must keep the frequency of the load voltage be constant, so, the reference value frequency is used to evaluate the angular synchronous speed $\left(\omega_{\bar{u}_s}^*\right)$ which then be integrated to calculate the synchronous angle $\left(\theta_{\bar{u}_s}^*\right)$. After that, the angle $\left(\theta_{\bar{u}_{s,k+1}}\right)$ can be evaluated through the following formula:

$$\theta_{\bar{u}_{s,k+1}} = \theta_{\bar{u}_{s,k}} + \left(\frac{\theta_{\bar{u}_{s,k}} - \theta_{\bar{u}_{s,k-1}}}{\Delta T}\right) T_s \quad (30)$$

The position of the rotor denoted by $\left(\theta_{me,k+1}\right)$, and can be expressed by:

$$\theta_{me,k+1} = \theta_{me,k} + \left(\frac{\theta_{me,k} - \theta_{me,k-1}}{\Delta T}\right) T_s \quad (31)$$

The Taylor expansion is used here to find the actual components of the predicted rotor current $\left(i_{dr,k+1}^{sv} \text{and} i_{qr,k+1}^{sv}\right)$ through the following formulations:

$$i_{dr,k+1}^{sv} = i_{dr,k}^{sv} + \left(\frac{di_{dr,k}^{sv}}{dt}\right) T_s \quad (32)$$

$$i_{qr,k+1}^{sv} = i_{qr,k}^{sv} + \left(\frac{di_{qr,k}^{sv}}{dt}\right) T_s \quad (33)$$

The components $\left(\frac{di_{dr,k}^{sv}}{dt} \text{and} \frac{di_{qr,k}^{sv}}{dt}\right)$ can be evaluated by using equations (21) and (22). In the same manner, we can find the actual components of the predicted stator current $\left(i_{ds,k+1}^{sv} and i_{qs,k+1}^{sv}\right)$. Subsequently, the actual value of the predicted torque $\left(T_{em,k+1}\right)$ as follows:

$$T_{em,k+1} = 1.5pL_m\left(i_{dr,k+1}^{sv} i_{qs,k+1}^{sv} - i_{qr,k+1}^{sv} i_{ds,k+1}^{sv}\right) \quad (34)$$

The actual value of the rotor flux $\left|\bar{\Psi}_{r,k+1}^{sv}\right|$ is found using the following formula:

$$\left|\bar{\Psi}_{r,k+1}^{sv}\right| = \sqrt{\left(\Psi_{dr,k+1}^{sv}\right)^2 + \left(\Psi_{qr,k+1}^{sv}\right)^2} \quad (35)$$

Where

$$\Psi_{dr,k+1}^{sv} = L_r i_{dr,k+1}^{sv} + L_m i_{ds,k+1}^{sv} \quad (36)$$

$$\Psi_{qr,k+1}^{sv} = L_r i_{qr,k+1}^{sv} + L_m i_{qs,k+1}^{sv} \quad (37)$$

The reference value of the torque $\left(T_{em,k+1}^*\right)$ can be expressed by:

$$T_{em,k+1}^* = 1.5pL_m\left(i_{dr,k}^* i_{qs,k}^* - i_{qr,k}^* i_{ds,k}^*\right) \quad (38)$$

Finally, the reference component of the rotor flux $\left|\bar{\Psi}_{r,k+1}^*\right|$ is calculated through this formulation:

$$\left|\bar{\Psi}_{r,k+1}^*\right| = \sqrt{\left(\Psi_{dr,k+1}^*\right)^2 + \left(\Psi_{qr,k+1}^*\right)^2} \quad (39)$$

Where

$$\Psi_{dr,k+1}^* = L_r i_{dr,k+1}^* + L_m i_{ds,k+1}^* \quad (40)$$

$$\Psi_{qr,k+1}^* = L_r i_{qr,k+1}^* + L_m i_{qs,k+1}^* \quad (41)$$

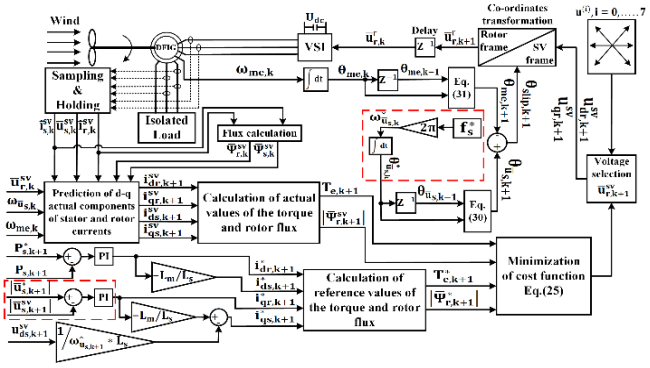

Fig. 3. Scheme of MPDTC approach for the DFIG

B. MPCC Technique

MPCC uses a simple cost function, as it does not require a weighting factor because its cost function made up of two comparable elements, the errors between the reference and actual values of the rotor current. The actual rotor current components $i_{dr,k+1}^{sv}$ and $i_{qr,k+1}^{sv}$ can be predicted using Taylor expansion, while the reference values of the rotor current $i_{dr,k+1}^{*}$ and $i_{qr,k+1}^{*}$ can be directly obtained using the errors of the load active power and load voltage with the aid of two PI regulators as mentioned previously [38].

The d-q actual components of the rotor current can be obtained using (32) and (33) after substituting for rotor current derivatives from (21) and (22).

The difference between the reference and actual values of the load active power is fed to a PI regulator which obtains $i_{dr,k+1}^{*}$, while the difference between the reference and actual values of the load voltage is fed to another PI regulator which obtains $i_{qr,k+1}^{*}$.

Lastly, after obtaining the d-q reference and actual rotor current components, they are fed to the adopted cost function which can be represented by:

$$\Lambda^{i} = \left|i_{dr,k+1}^{*} - i_{dr,k+1}^{sv}\right|^{i} + \left|i_{qr,k+1}^{*} - i_{qr,k+1}^{sv}\right|^{i} \tag{42}$$

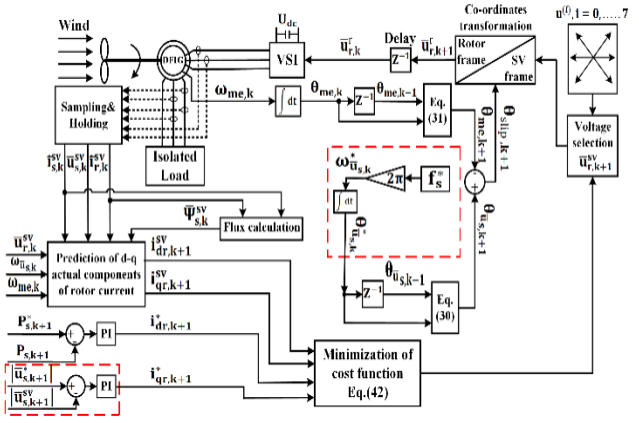

Fig. 4. Scheme of MPCC approach for the DFIG

C. Proposed Predictive Voltage Control (PVC)Technique

The proposed cost function which utilized in our proposed algorithm can be expressed by:

$$C^{i} = \left|u_{dr,k+1}^{*} - u_{dr,k+1}^{sv}\right|^{i} + \left|u_{qr,k+1}^{*} - u_{qr,k+1}^{sv}\right|^{i} \tag{43}$$

As it's clear from (43), the adopted cost function is complication free; as its function is to minimize the error value between the reference and predicted actual values of the d-q components of the rotor voltage, so its components are analogous, thus it doesn't require a weighting factor which can cause a problem of mismatch as in case of MPDTC. Furthermore, the cost function is free of variables which are obtained through the model parameters, which leads to handling the issue of system uncertainties.

Fig. 5, outlines the configuration of the proposed PVC, in which the actual values of the predicted rotor voltage $\left(u_{dr,k+1}^{sv} \text{and } u_{qr,k+1}^{sv}\right)$, which are obtained directly through the switching states of the voltage source inverter (VSI), meanwhile, the reference components of the rotor voltage $\left(u_{dr,k+1}^{*} \text{and } u_{qr,k+1}^{*}\right)$ can be calculated by the following equations:

$$u_{dr,k+1}^{*} = R_r i_{dr,k+1}^{*} + \frac{d\Psi_{dr,k+1}^{sv}}{dt} - \omega_{slip,k+1}\Psi_{qr,k+1}^{*} \tag{44}$$

$$u_{qr,k+1}^{*} = R_r i_{qr,k+1}^{*} + \frac{d\Psi_{qr,k+1}^{sv}}{dt} + \omega_{slip,k+1}\Psi_{dr,k+1}^{*} \tag{45}$$

Where the derivative d-q components of the rotor flux are obtained as follows:

$$\frac{d\Psi_{dr,k+1}^{sv}}{dt} = \frac{\Psi_{dr,k+1}^{*} - \Psi_{dr,k}}{T_s} \tag{46}$$

$$\frac{d\Psi_{qr,k+1}^{sv}}{dt} = \frac{\Psi_{qr,k+1}^{*} - \Psi_{qr,k}^{sv}}{T_s} \tag{47}$$

The components $\left(\Psi_{dr,k} \text{ and } \Psi_{qr,k}^{sv}\right)$ are evaluated using (17) and (18), meanwhile the calculation of the reference rotor flux components $\left(\Psi_{dr,k+1}^{*} \text{ and } \Psi_{qr,k+1}^{*}\right)$ will be described in a systematic manner as following:

Under stator filed orientation (SFO), and steady state operation of the DFIG, we can deduce the following relations:

$$\Psi_{ds,k+1}^{sf} = \left|\bar{\Psi}_{s,k+1}^{sf}\right| \quad \text{and} \quad \Psi_{qs,k+1}^{sf} = 0.0 \tag{48}$$

$$u_{ds,k+1}^{sf} \approx 0.0 \quad \text{and} \quad u_{qs,k+1}^{sf} \approx \left|\bar{u}_{s,k+1}^{sf}\right| \tag{49}$$

As mentioned in [31], the variation of the rotor flux can be represented as follows:

$$\frac{d\bar{\Psi}_{r,k+1}^{sf}}{dt} = \frac{L_r L_t}{R_r L_m - L_r L_t}\left[\frac{R_r}{L_t}\frac{d\bar{\Psi}_{s,k+1}^{sf}}{dt} - \bar{u}_{r,k+1}^{sf} + j\left(\omega_{\bar{\Psi}_{s,k+1}} - \omega_{me,k+1}\right)\bar{\Psi}_{r,k+1}^{sf}\right] \tag{50}$$

After that, by performing the Laplace transformation to (50), it results in:

$$\bar{\Psi}_{r,k+1}^{sf}(S) = \frac{L_r R_r S\bar{\Psi}_{s,k+1}^{sf}(S) - L_r L_t \bar{u}_{r,k+1}^{sf}(S)}{(R_r L_m - L_r L_t) - jL_r L_t\left(\omega_{\bar{\Psi}_{s,k+1}} - \omega_{me,k+1}\right)} \tag{51}$$

The time constant of the rotor flux is denoted by (T_f), and can be defined by:

$$T_f = R_r L_m - L_r L_t \tag{52}$$

The magnitude of the stator flux can be obtained as follows:

$$\begin{aligned}\left|\bar{\Psi}^{sf}_{s,k+1}\right| = \Psi^{sf}_{ds,k+1} &= \frac{u^{sf}_{qs,k+1}}{\omega_{\bar{\Psi}\,s,k+1}} = \frac{\left|\bar{u}^{sf}_{s,k+1}\right|}{\omega_{\bar{\Psi}\,s,k+1}} \\ &= \frac{380}{2 * \pi * 50} = 1.2\ Vs\end{aligned} \tag{53}$$

The vectors of the stator and rotor fluxes can be represented in the exponential form as following:

$$\bar{\Psi}^{sf}_{s,k+1} = \left|\bar{\Psi}^{sf}_{s,k+1}\right| e^{j\omega_{\bar{\Psi}\,s,k+1} t} \tag{54}$$

$$\bar{\Psi}^{sf}_{r,k+1} = \left|\bar{\Psi}^{sf}_{r,k+1}\right| e^{j\omega_{me,k+1} t} \tag{55}$$

With the aid of (54) and (55), we can represent the electromagnetic torque of the DFIG by:

$$\begin{aligned}T_{em,k+1} = 1.5p \frac{L_m}{L_r L_t} &\left|\bar{\Psi}^{sf}_{s,k+1}\right| e^{j\omega_{\bar{\Psi}\,s,k+1} t} \\ &\times \left|\bar{\Psi}^{sf}_{r,k+1}\right| e^{j\omega_{me,k+1} t}\end{aligned} \tag{56}$$

Where × refers to the cross product. Consequently, using (53) and (56), we can express the torque by:

$$\begin{aligned}T_{em,k+1} = 1.2 * 1.5p \frac{L_m T_f}{L_r L_t} &\left|\bar{\Psi}^{*}_{r,k+1}\right| \left(1 - e^{\frac{-t}{T_f}}\right) \\ &* \left(\underbrace{\omega_{\bar{\Psi}\,s,k+1} - \omega_{me,k+1}}_{\omega_{slip,k+1}}\right)\end{aligned} \tag{57}$$

The component $\left|\bar{\Psi}^{*}_{r,k+1}\right|$ can be obtained as follows:

$$\left|\bar{\Psi}^{*}_{r,k+1}\right| = \frac{L_m}{L_s}\left|\bar{\Psi}^{*}_{s,k+1}\right| + \sigma L_r \left|\bar{\imath}^{*}_{r,k+1}\right| \tag{58}$$

Where, the component $\left|\bar{\Psi}^{*}_{s,k+1}\right|$ can be obtained using (52).

As it's obvious from (57), the DFIG's torque can be controlled via regulating the angular slip frequency $(\omega_{slip,k+1})$, with keeping the stator and rotor flux magnitudes constant. Therefore, there will be a reference value of the angular slip speed $(\omega^{*}_{slip,k+1})$, for any value of the reference torque $(T^{*}_{em,k+1})$. After that, the obtained values of $(\omega^{*}_{slip,k+1})$ are used to calculate the values of $\left(\omega^{*}_{\bar{\Psi}_{s,k+1}}\right)$, which are then utilized to evaluate the rotor flux components $(\Psi^{*}_{\alpha r,k+1}$ and $\Psi^{*}_{\beta r,k+1})$, which are then transferred into synchronous frame and utilized by (44) and (45) to obtain the d-q reference components of the rotor voltage $(u^{*}_{dr,k+1}$ and $u^{*}_{qr,k+1})$.

The design of the PI torque regulator which will be used to find $(\omega^{*}_{slip,k+1})$ can be performed in the following manner:

As noticed from (57), we can consider term $K = 1.2 * 1.5p \frac{L_m T_f}{L_r L_t}\left|\bar{\Psi}^{*}_{r,k+1}\right|$ as a constant value, then we differentiate (57) with respect to the time, which results:

$$\frac{dT_{em,k+1}}{dt} = K * \omega^{*}_{slip,k+1} * \frac{1}{T_f} e^{\frac{-t}{T_f}} \tag{59}$$

After that, by implementing the Laplace transformation to (59), it results:

$$S T_{em,k+1}(S) - T_{em,k+1}(0) = \frac{K}{T_f} \frac{1}{S + \frac{1}{T_f}} \omega^{*}_{slip,k+1}(S) \tag{60}$$

With assuming zero initial torque, we get:

$$\omega^{*}_{slip,k+1}(S) = \frac{T_f}{K}\left(S + \frac{1}{T_f}\right) * S T_{em,k+1}(S) \tag{61}$$

$$\frac{T_{em,k+1}(S)}{\omega^{*}_{slip,k+1}(S)} = \frac{K}{T_f S^2 + S} \tag{62}$$

We can express the transfer function of the of the PI torque regulator as follows:

$$\omega^{*}_{slip,k+1}(S) = \overbrace{\left(k_p + \frac{k_i}{S}\right)}^{PI} \overbrace{\left[T^{*}_{em,k+1}(S) - T_{em,k+1}(S)\right]}^{Torque\ error} \tag{63}$$

By dividing both sides of (63) by $\{T_{em,k+1}(S)\}$, it results in:

$$\frac{\omega^{*}_{slip,k+1}(S)}{T_{em,k+1}(S)} = \left(k_p + \frac{k_i}{S}\right)\left[\frac{T^{*}_{em,k+1}(S)}{T_{em,k+1}(S)} - 1\right] \tag{64}$$

By substituting the component $\{\omega^{*}_{slip,k+1}(S)\}$ from (62) into (64), we can deduce that:

$$\begin{aligned}&\frac{T_{e,k+1}(S)}{T_{e,k+1}(S)}\left(\frac{T_f S^2 + S}{K}\right) = \left(k_p + \frac{k_i}{S}\right)\left[\frac{T^{*}_{em,k+1}(S)}{T_{em,k+1}(S)} - 1\right] \\ &\frac{T_f S^2 + S}{K} = \left(\frac{k_p S + k_i}{S}\right)\left[\frac{T^{*}_{em,k+1}(S)}{T_{em,k+1}(S)}\right] - \left(\frac{k_p S + k_i}{S}\right) \\ &\left(\frac{k_p S + k_i}{S}\right)\left[\frac{T^{*}_{em,k+1}(S)}{T_{em,k+1}(S)}\right] = \frac{k_p S + k_i}{S} + \frac{T_f S^2 + S}{K} \\ &\frac{T^{*}_{em,k+1}(S)}{T_{em,k+1}(S)} = \frac{T_f S^3 + S^2 + K k_p S + K k_i}{K k_p S + K k_i} \\ &\frac{T_{em,k+1}(S)}{T^{*}_{em,k+1}(S)} = \frac{K k_p S + K k_i}{T_f S^3 + S^2 + K k_p S + K k_i}\end{aligned} \tag{65}$$

The denominator of both (65) represents the characteristic equation, which controls the dynamics of the PI torque regulator, it can be reformulated as:

$$S^3 + \frac{1}{T_f} S^2 + \frac{K k_p}{T_f} S + \frac{K k_i}{T_f} = 0.0 \tag{66}$$

For third order systems, the characteristic equation can be defined by:

$$S^3 + 2D\omega_n S^2 + \omega_n S + \frac{\omega_n^2}{4D^2} = 0 \tag{67}$$

Finally, we can easily determine the parameters $(k_p$ and $k_i)$ of the PI torque controller by comparing (65) and (66), the comparison reveals that:

$$k_p = \frac{T_f}{K}\omega_n \quad \text{and} \quad k_i = \frac{T_f}{4KD^2}\omega_n^2 \tag{68}$$

Now, the PI is used to obtain $(\omega^*_{slip,k+1})$, which is then utilized to find $(\omega^*_{\bar{\Psi}_{s,k+1}})$, which is then integrated to find $(\theta^*_{\bar{\Psi}_{s,k+1}})$ to be used in calculating the rotor flux components $(\Psi^*_{\alpha r,k+1}$ and $\Psi^*_{\beta r,k+1})$ as follows:

$$\Psi^*_{\alpha r,k+1} = \left|\bar{\Psi}^*_{r,k+1}\right| * \cos\left(\theta^*_{\bar{\Psi}_{s,k+1}}\right) \tag{69}$$

$$\Psi^*_{\beta r,k+1} = \left|\bar{\Psi}^*_{r,k+1}\right| * \sin\left(\theta^*_{\bar{\Psi}_{s,k+1}}\right) \tag{70}$$

After that, the rotor flux components are represented in synchronous frame, and then used to obtain the reference voltage components $(u^*_{dr,k+1}$and$u^*_{qr,k+1})$, using (44) and (45).

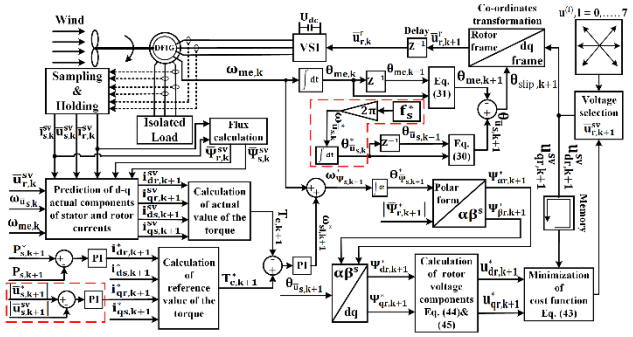

Fig. 5. Scheme of proposed PVC approach for the DFIG

IV. TEST RESULTS

The tests were performed utilizing MATLAB simulation (Simulink). The dynamic performance of the DFIG was tested under two different control algorithms, which are the MPDTC methodology and the proposed PVC technique. As shown in Fig. 6, the DFIG has variable operating speeds, as it was driven by a wind turbine. The generator supplies an isolated load which is three phase induction motor, which described in Table A3, meanwhile the parameters of the DFIG and wind turbine are introduced in Table A1 and Table A2, respectively.

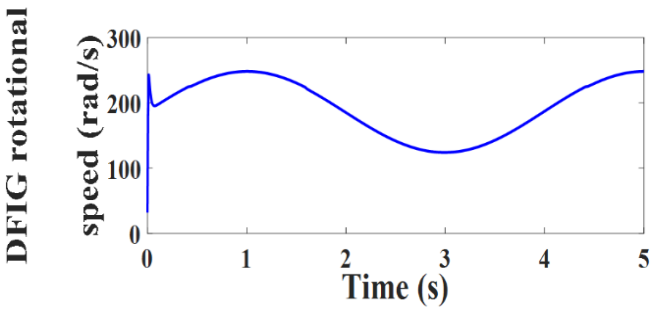

Fig. 6. Wind turbine operating speeds (rad/s)

A. Testing with MPDTC Strategy

The performance of the DFIG was tested under MPDTC methodology [12, 19] to study the dynamic performance of the generator and compare it with the formulated predictive controller. The obtained results are shown in Figs. 7-15, which show that the actual values follow their reference values with some ripples.

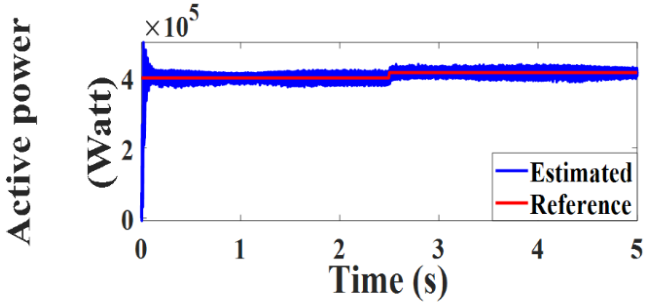

Fig. 7. Active power with MPDTC (Watt)

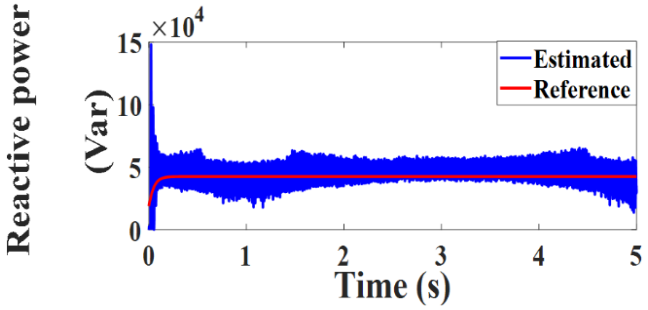

Fig. 8. Reactive power with MPDTC (Var)

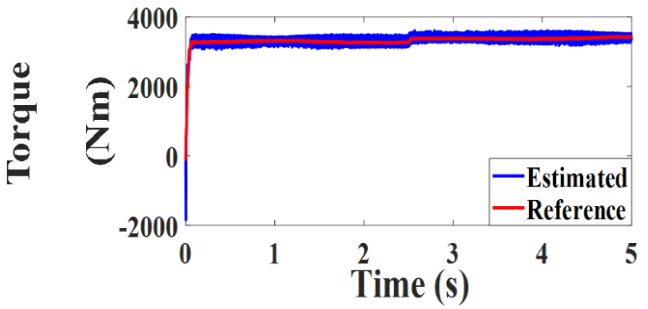

Fig. 9. Developed torque with MPDTC (Nm)

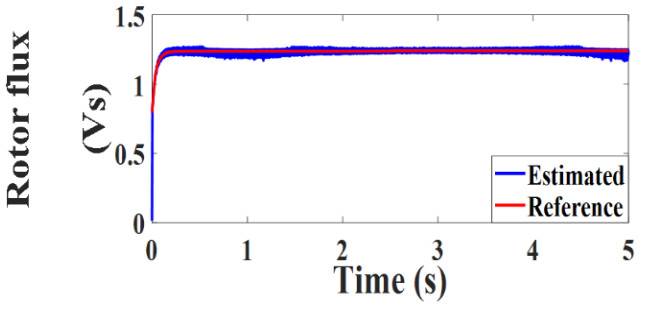

Fig. 10. Rotor flux with MPDTC (Vs)

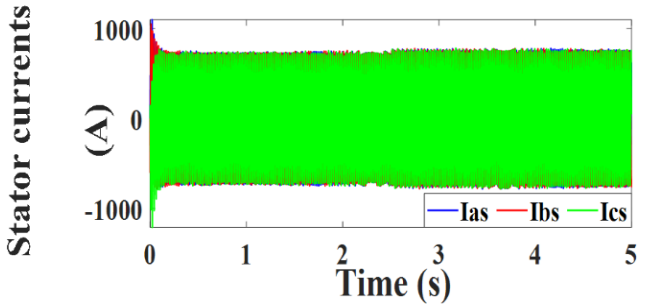

Fig. 11. Stator currents with MPDTC (A)

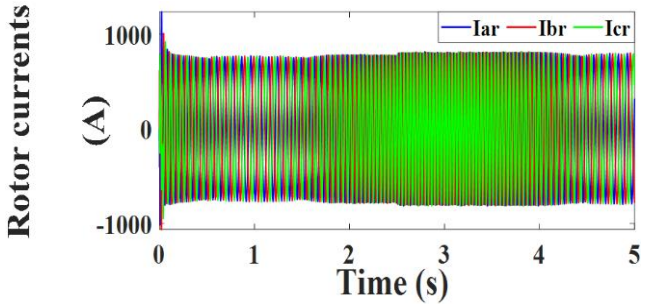

Fig. 12. Rotor currents with MPDTC (A)

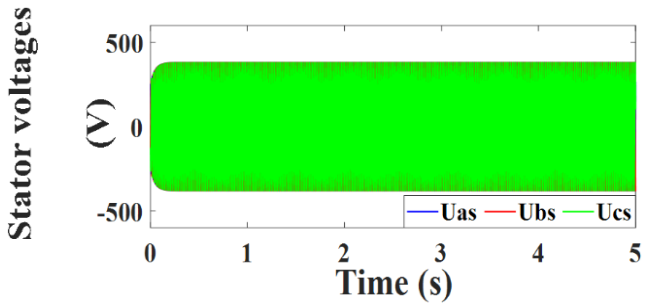

Fig. 13. Stator voltage components with MPDTC (V)

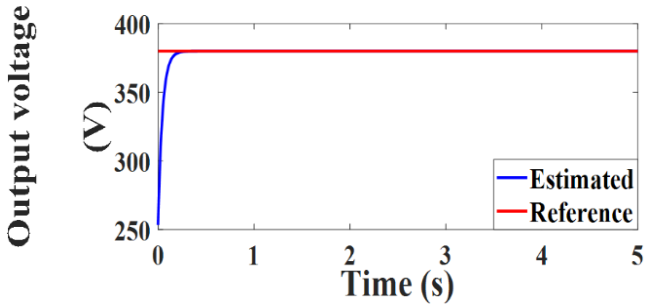

Fig. 14. Load voltage with MPDTC (V)

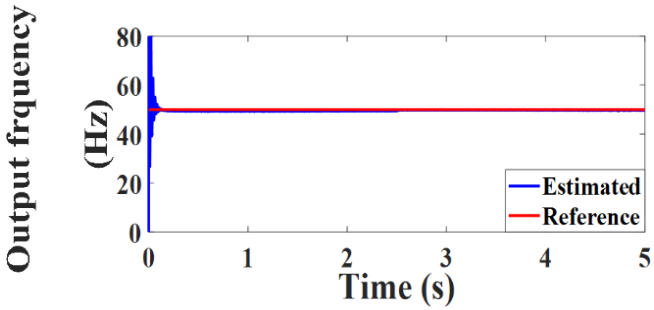

Fig. 15. Frequency of load voltage with MPDTC (Hz)

B. Testing with MPCC Strategy [38]

Tests for the DFIG's performance ware performed under the MPCC algorithm and the obtained results are shown in Figs. 16-24, which clarify that the actual values follow their reference values. The results show that the dynamic response of the MPCC is slower than that of MPDTC, but on the other side, the ripples' content is reduced.

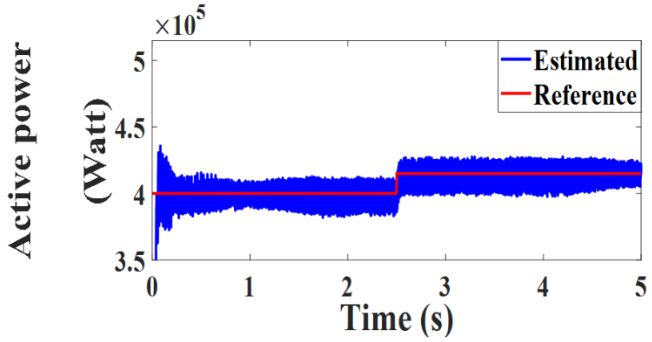

Fig. 16. Active power with MPCC (Watt)

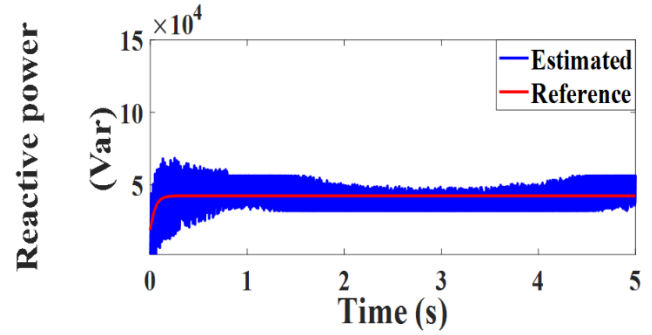

Fig. 17. Reactive power with MPCC (Watt)

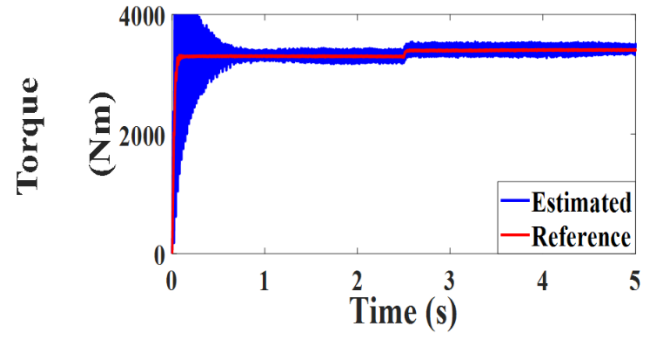

Fig. 18. Developed torque with MPCC (Nm)

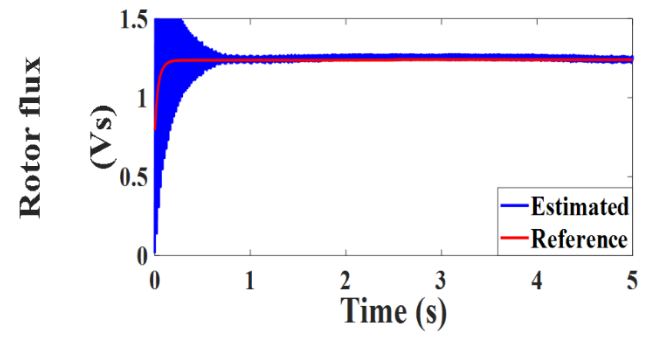

Fig. 19. Rotor flux with MPCC (Vs)

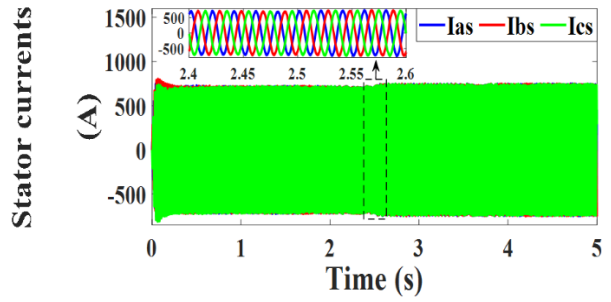

Fig. 20. Stator currents with MPCC (A)

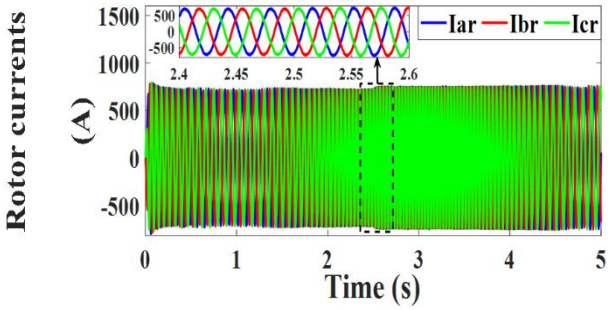

Fig. 21. Rotor currents with MPCC (A)

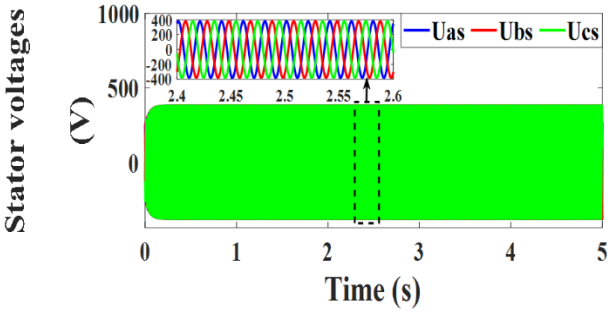

Fig. 22. Stator voltage components with MPCC (V)

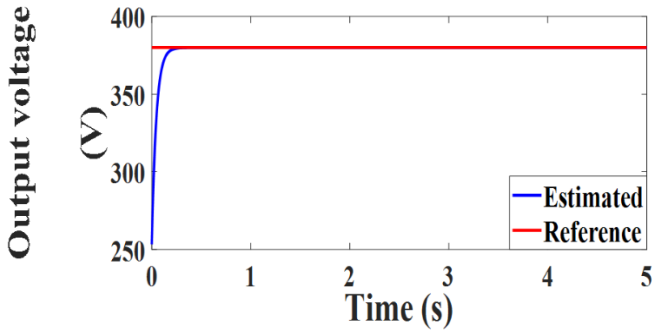

Fig. 23. Load voltage with MPCC (V)

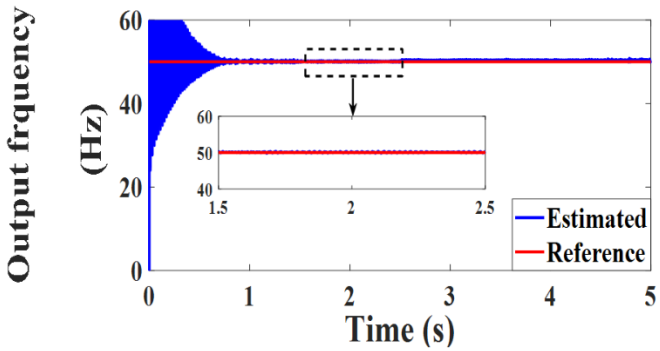

Fig. 24. Frequency of load voltage with MPDTC (Hz)

C. *Testing with Proposed PVC Strategy*

The DFG's dynamic performance was studied under the propose PVC scheme to prove the ability of the formulated controller to handle the wind changes and enhance the performance of the DFIG. The test results are introduced in Figs. 25-33. The results reveal that the designed controller has succeeded in achieving its targets, as the actual values of the active power, reactive power, developed torque and rotor flux track their reference values with high precision and lower ripples' content compared to MPDTC. Furthermore, The DFIG under the designed scheme could provide a constant output voltage with constant frequency even under wind changes, which is considered as a principal requirement for standalone systems. As it's obvious from the obtained results, the formulated controller has successfully improved the dynamic response of DFIG and made it faster than that of MPDTC technique.

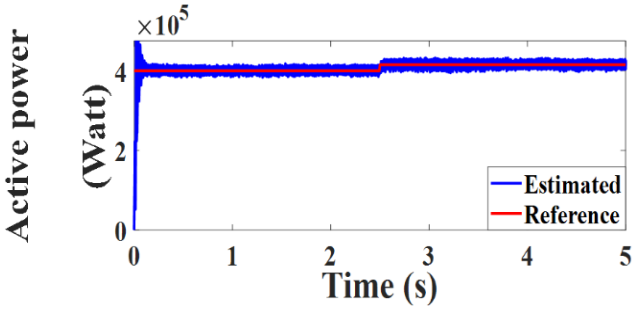

Fig. 25. Active power with PVC (Watt)

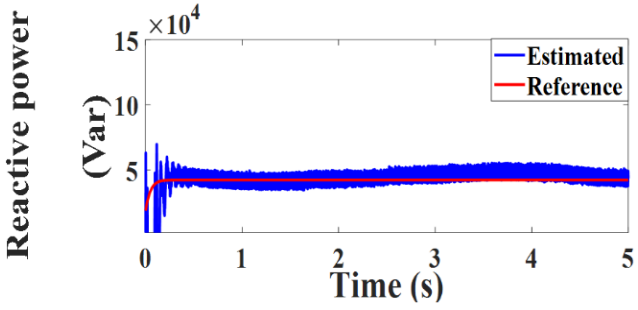

Fig. 26. Reactive power with PVC (Var)

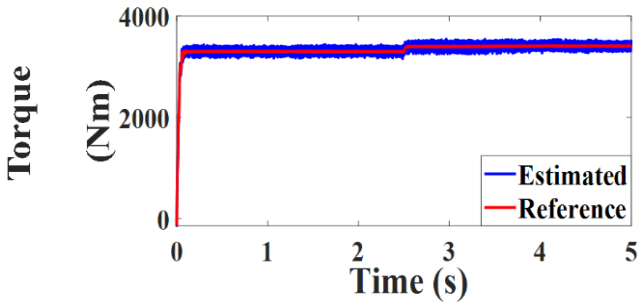

Fig. 27. Developed torque with PVC (Nm)

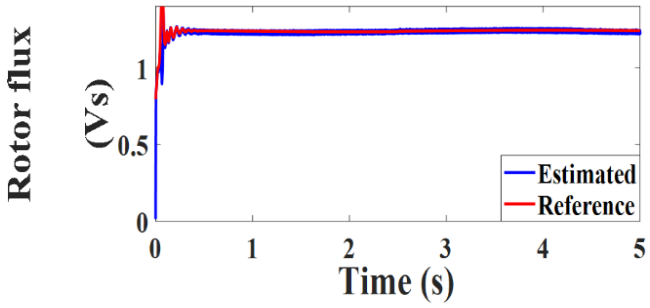

Fig. 28. Rotor flux with PVC (Vs)

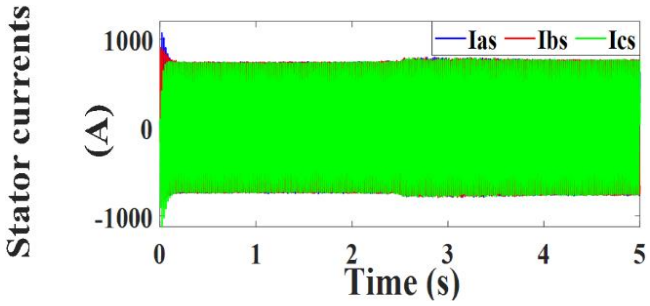

Fig. 29. Stator currents with PVC (A)

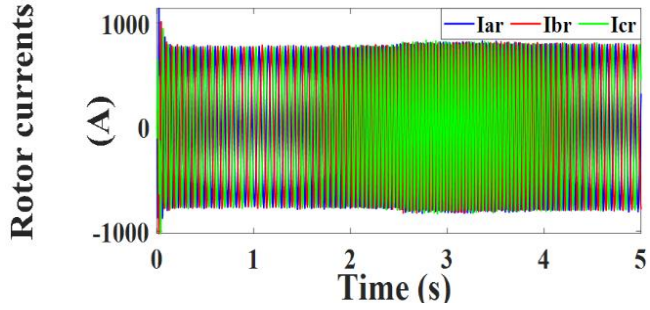

Fig. 30. Rotor currents with PVC (A)

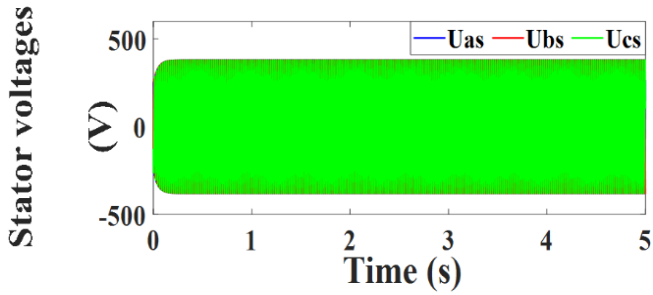

Fig. 31. Stator voltage components with PVC (V)

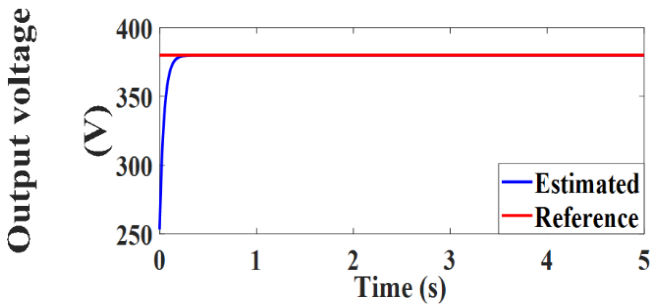

Fig. 32. Load voltage with PVC (V)

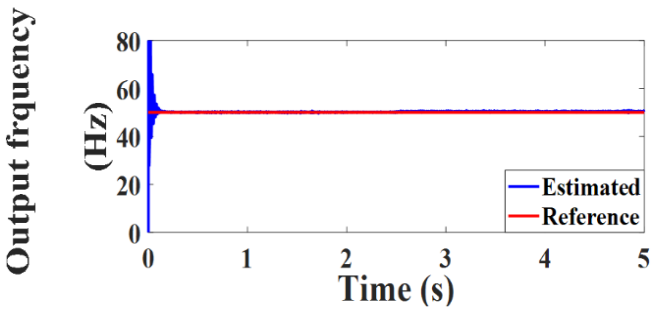

Fig. 33. Frequency of load voltage with PVC (Hz)

D. Comparison Study

After testing and studying the performance of the DFIG under each algorithm individually, we preferred to perform a comprehensive and detailed comparison for the DFIG's performance under MPDTC [12, 19], MPCC [38], and our formulated controller, so we can easily define the advantages and shortages of each control scheme to be able to easily determine the most appropriate methodology to be utilized with the DFIG. The comparison has been performed in terms of time of time of dynamic response, content of ripples, number of executed commutations, and total harmonic distortion (THD). The results of the comparison are presented in Figs. 34-37. The obtained results reveal that the proposed PVC algorithm has a faster dynamic response than that of MPDTC and MPCC, as it takes lower time to reach to the required reference value, which is also evident in Table I. Furthermore, Table II, clarifies that our designed controller can minimize the content of ripples remarkably compared to MPDTC and MPCC methods. Moreover, the proposed algorithm introduces less computational burden, as it has lower number of executed commutations compared with that of MPDTC and MPCC strategies, as shown in Table III.

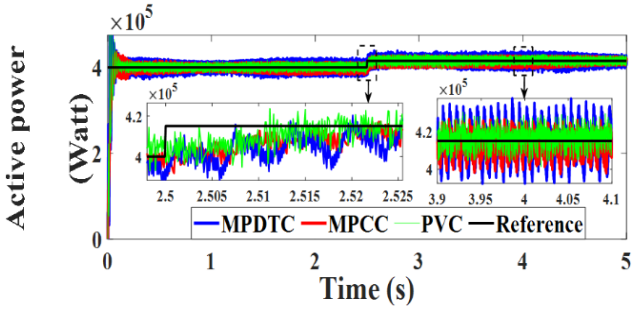

Fig. 34. Active power (Watt)

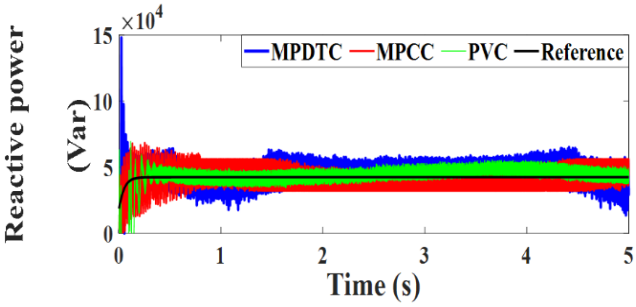

Fig. 35. Reactive power (Var)

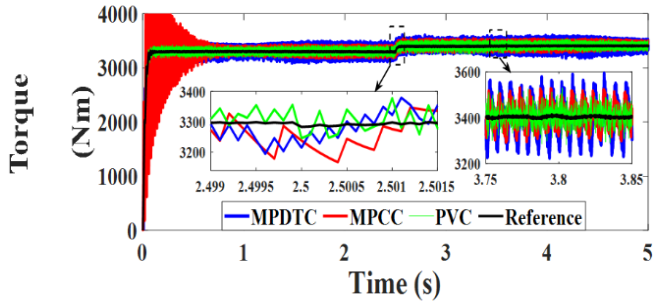

Fig. 36. Developed torque (Nm)

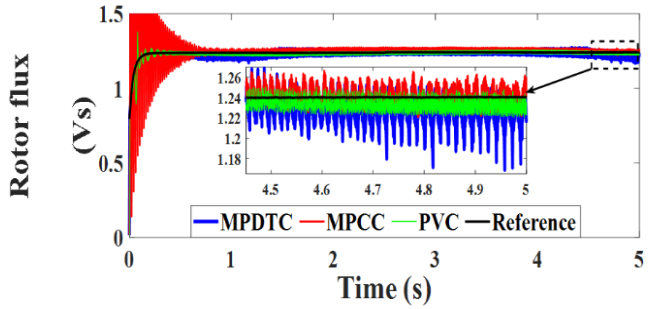

Fig. 37. Rotor flux (Vs)

TABLE I. DYNAMIC RESPONSE TIME TAKEN BY THE ACTUAL VALUES TO TRACK THEIR REFERENCES

Technique	Time taken by the active power profile (ms)	Time taken by the torque profile (ms)
MPDTC	15	0.5
MPCC	20	1.2
PVC	11	0.2

TABLE II. RIPPLES' CONTENT OF THE ACTUAL VALUES ABOVE THEIR REFERENCES

Algorithm	Ripples of active power (Watt)	Ripples of reactive power (Var)	Ripples of developed torque (Nm)	Ripples of rotor flux (Vs)
MPDTC	22300	20350	189	0.031
MPCC	15600	13820	108	0.02
PVC	9800	5610	61	0.009

TABLE III. COMPARISON IN TERMS OF COMMUTATIONS EXECUTED BY THE PREDICTIVE CONTROLLERS

Technique	No. of commutations
MPDTC	3856
MPCC	4087
Proposed PVC	2412

The fast Fourier transform (FFT) analysis for the components of the stator current under the MPDTC[12, 19], MPCC [38], and our formulated PVC are presented in Fig. 38-46. The THD of the designed PVC is lower than that of MPDTC and MPCC as it's clear from comparing the current spectrums and also confirmed through the numerical values which presented in Table IV.

Eventually, it can be deduced that, the proposed PVC scheme is the best selection for using with the DFIG, as it obviated the main defects which faced other classic controllers and succeeded in improving the dynamic performance of the generator, as explained in details.

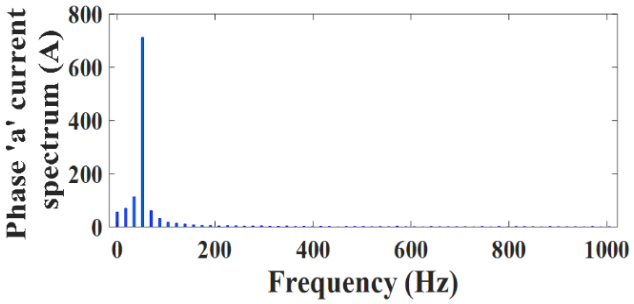

Fig. 38. Spectrum of Phase "a" of stator current under MPDTC

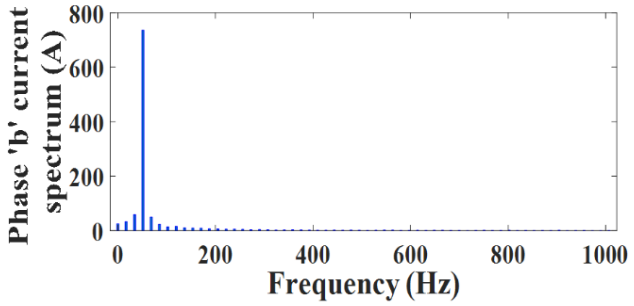

Fig. 39. Spectrum of Phase "b" of stator current under MPDTC

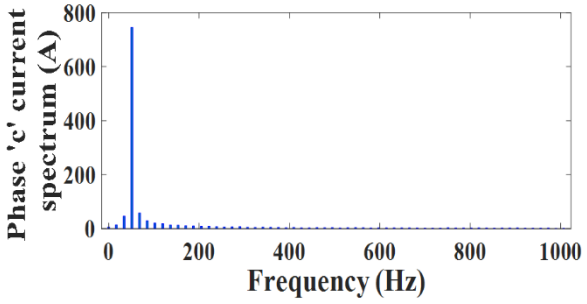

Fig. 40. Spectrum of Phase "c" of stator current under MPDTC

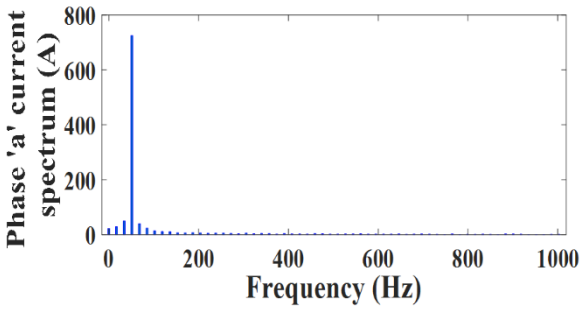

Fig. 41. Spectrum of Phase "a" of stator current under MPCC

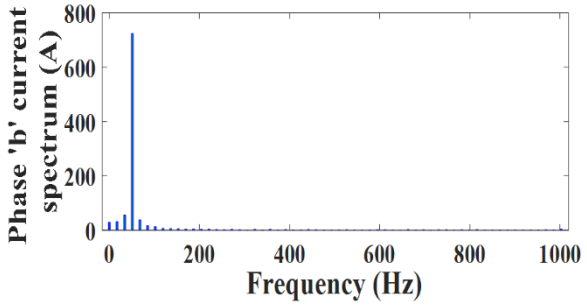

Fig. 42. Spectrum of Phase "b" of stator current under MPCC

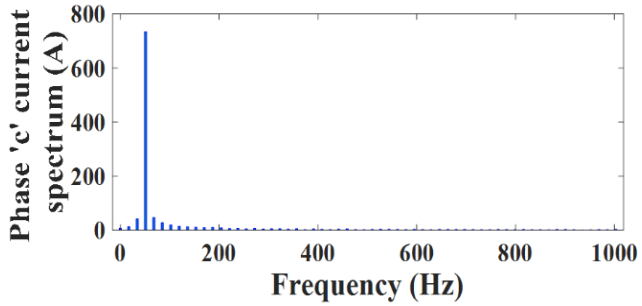

Fig. 43. Spectrum of Phase "c" of stator current under MPCC

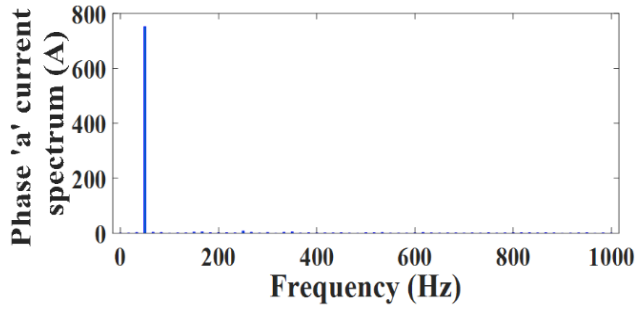

Fig. 44. Spectrum of Phase "a" of stator current under PVC

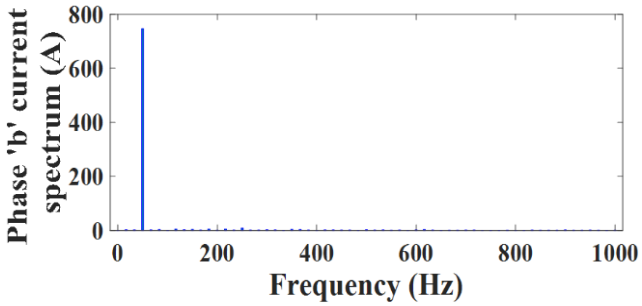

Fig. 45. Spectrum of Phase "b" of stator current under PVC

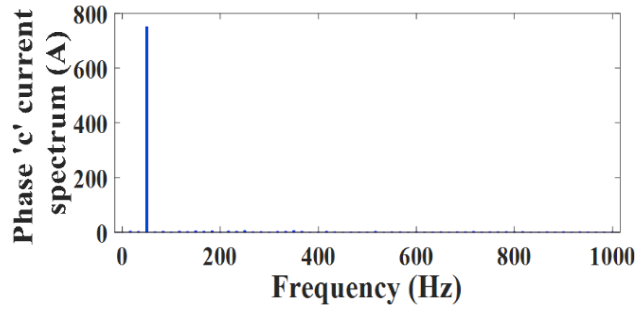

Fig. 46. Spectrum of Phase "c" of stator current under PVC

TABLE IV. FFT ANALYSIS FOR THE STATOR CURRENT COMPONENTS

		Phase A	Phase B	Phase C
MPDTC	**Fundamental**	712.155 A	736.363 A	745.412 A
	THD	3.02 %	2.92 %	4.11 %
MPCC	**Fundamental**	725.288 A	724.037 A	734.196 A
	THD	2.78 %	2.15 %	3.85 %
PVC	**Fundamental**	751.477 A	746.606 A	750.4 A
	THD	1.08 %	1.06 %	1.23 %

V. CONCLUSIONS

The present article has introduced a detailed analysis for the dynamic performance of the doubly fed induction generator (DFIG) which driven by a wind turbine and studied the effect of wind changes on the performance of the generator under three different control schemes: model predictive direct torque control (MPDTC), model predictive current control (MPCC)approaches as classic methods of control and a newly efficient designed predictive voltage control (PVC) algorithm as an improved methodology of control. The formulated controller has a very simple cost function compared to MPDTC and MPCC, as it doesn't utilize a weighting factor value, in addition its terms don't need be estimated which minimizes the calculation time, which leads to make this controller more efficient and robustness against uncertainties. A comprehensive and detailed comparison has been performed for the DFIG's performance under MPDTC, MPCC and the designed controller. The obtained results prove the validation and superiority of our formulated predictive controller, as it has managed to attain the control goals and obviating the shortages of other control approaches. The proposed PVC scheme has succeeded in enhancing the dynamic performance of the DFIG remarkably through introducing the fastest dynamic response, reducing the ripples' content, minimizing the THD and reducing the number of performed commutations and thus reducing the computational burden. In the near future, we will study the analysis of the fault tolerance control of the wind driven standalone DFIG.

APPENDIX A

TABLE A1. DATA OF THE DFIG

Parameter	**Value**	**Parameter**	**Value**
Rated power	1.5 MW	Rated stator voltage	380 V
Rs	70 mΩ	J_g	0.3125 kg.m^2
Rr	87 mΩ	Operating frequency	50 Hz
Ls	16.25 mH	Sampling time	100 µs
Lr	16.3 mH	K_p and K_i (Active power regulator)	0.0001 and -0.1
Lm	16 mH	K_p and K_i (Stator voltage regulator)	0.01 and -20
Pole pairs (p)	3		

TABLE A2. DATA OF THE WIND TURBINE

Parameter	**Value**	**Parameter**	**Value**
Rated power	1.5 MW	$C_{p,max}$	0.51
r	35.25 m	λ_{opt}	8.1
J_t	1000 kg.m2	G	90

TABLE A3. PARAMETERS OF THE LOAD (IM)

Parameter	**Value**	**Parameter**	**Value**
Rated power	50 Kw	Lm	0.654mH
Rs	0.08 Ω	Pole pairs (p)	3
Rr	0.234 Ω	Inertia	1.662 kg.m2
Ls	0.955mH	T_{rated}	498 Nm
Lr	0.955mH	N_{rated}	960 rpm

REFERENCES

[1] N. L. Panwar, S. C. Kaushik, and S. Kothari, "Role of renewable energy sources in environmental protection: A review," *Renewable and Sustainable Energy Reviews*, vol. 15, no. 3, pp. 1513-1524, 2011/04/01/ 2011.

[2] J. R. Andrade and R. J. Bessa, "Improving Renewable Energy Forecasting With a Grid of Numerical Weather Predictions," *IEEE Transactions on Sustainable Energy*, vol. 8, no. 4, pp. 1571-1580, 2017.

[3] A. Zhour, G. Sihem, D. J. I. J. o. R. Djalel, and C. Systems, "A New Approach to Fault Detection in the Power Converter in Wind Turbine Conversion Systems," *International Journal of Robotics and Control Systems*, vol. 1, no. 4, pp. 428-439, 2021.

[4] C. Nagarajan, B. Tharani, S. Saravanan, R. J. I. J. o. R. Prakash, and C. Systems, "Performance Estimation and Control Analysis of AC-DC/DC-DC Hybrid Multi-Port Intelligent Controllers Based Power Flow Optimizing Using STEM Strategy and RPFC Technique," *International Journal of Robotics and Control Systems*, vol. 2, no. 1, pp. 124-139, 2022.

[5] M. A. Mossa, O. Gam, N. Bianchi and N. V. Quynh, "Enhanced Control and Power Management for a Renewable Energy-Based Water Pumping System," in *IEEE Access*, vol. 10, pp. 36028-36056, 2022.

[6] S. Puchalapalli, S. K. Tiwari, B. Singh, and P. K. Goel, "A Microgrid Based on Wind-Driven DFIG, DG, and Solar PV Array for Optimal Fuel Consumption," *IEEE Transactions on Industry Applications*, vol. 56, no. 5, pp. 4689-4699, 2020.

[7] L. Dambrosio and B. Fortunato, "One-step-ahead adaptive control of a wind-driven, synchronous generator system," *Energy*, vol. 24, no. 1, pp. 9-20, 1999/01/01/ 1999.

[8] L. A. C. Lopes and R. G. Almeida, "Wind-driven self-excited induction generator with voltage and frequency regulated by a reduced-rating voltage source inverter," *IEEE Transactions on Energy Conversion*, vol. 21, no. 2, pp. 297-304, 2006.

[9] M. M. Mahmoud, M. M. Aly, H. S. Salama, and A.-M. M. Abdel-Rahim, "Dynamic evaluation of optimization techniques–based proportional–integral controller for wind-driven permanent magnet synchronous generator," *Wind Engineering*, vol. 45, no. 3, pp. 696-709, 2021/06/01 2020.

[10] O. M. Kamel, M. A. Mossa, and A. A. Z. Diab, "Evaluating Dynamic Performance of DTC under Grid Disturbance for a Wind Driven DFIG," in *2019 21st International Middle East Power Systems Conference (MEPCON)*, 2019, pp. 213-219.

[11] M. A. Mossa and S. Bolognani, "High performance Direct Power Control for a doubly fed induction generator," in *IECON 2016 - 42nd Annual Conference of the IEEE Industrial Electronics Society*, 2016, pp. 1930-1935.

[12] M. A. Mossa, T. D. Do, A. S. Al-Sumaiti, N. V. Quynh, and A. A. Z. Diab, "Effective Model Predictive Voltage Control for a Sensorless Doubly Fed Induction Generator," *IEEE Canadian Journal of Electrical and Computer Engineering*, vol. 44, no. 1, pp. 50-64, 2021.

[13] C. M. R. Osorio, J. S. S. Chaves, A. L. L. F. Murari, and A. J. S. Filho, "Comparative Analysis of the Doubly Fed Induction Generator (DFIG) Under Balanced Voltage Sag Using a Deadbeat Controller," *IEEE Latin America Transactions*, vol. 15, no. 5, pp. 869-876, 2017.

[14] C. M. R. Charles, V. Vinod, and A. Jacob, "Field Oriented Control of DFIG Based Wind Energy System Using Battery Energy Storage System," *Procedia Technology*, vol. 24, pp. 1203-1210, 2016/01/01/ 2016.

[15] M. A. Mossa and Y. S. Mohamed, "Novel Scheme for Improving the Performance of a Wind Driven Doubly Fed Induction Generator during Grid Fault," *Wind Engineering*, vol. 36, no. 3, pp. 305-334, 2012/06/01 2012.

[16] R. A. J. Amalorpavaraj, P. Kaliannan, S. Padmanaban, U. Subramaniam, and V. K. Ramachandaramurthy, "Improved Fault Ride Through Capability in DFIG Based Wind Turbines Using Dynamic Voltage Restorer With Combined Feed-Forward and Feed-Back Control," *IEEE Access*, vol. 5, pp. 20494-20503, 2017.

[17] A. A. Hassan, Y. S. Mohamed, A. M. El-Sawy, and M. A. Mossa, "Control of a Wind Driven DFIG Connected to the Grid Based on Field Orientation," *Wind Engineering*, vol. 35, no. 2, pp. 127-143, 2011/04/01 2011.

[18] P. Pura and G. Iwański, "Rotor Current Feedback Based Direct Power Control of a Doubly Fed Induction Generator Operating with Unbalanced Grid," *Energies*, vol. 14, no. 11, 2021.

[19] M. A. Mossa, M. K. Abdelhamid, A. A. Hassan, and N. Bianchi, "Improving the Dynamic Performance of a Variable Speed DFIG for Energy Conversion Purposes Using an Effective Control System," *Processes*, vol. 10, no. 3, 2022.

[20] R. M. Prasad and M. A. Mulla, "Mathematical Modeling and Position-Sensorless Algorithm for Stator-Side Field-Oriented Control of Rotor-Tied DFIG in Rotor Flux Reference Frame," *IEEE Transactions on Energy Conversion*, vol. 35, no. 2, pp. 631-639, 2020.

[21] M. A. Mossa, O. Gam, and N. Bianchi, "Dynamic Performance Enhancement of a Renewable Energy System for Grid Connection and Stand-Alone Operation with Battery Storage," *Energies*, vol. 15, no. 3, 2022.

[22] A. Gundavarapu, H. Misra, and A. K. Jain, "Direct Torque Control Scheme for DC Voltage Regulation of the Standalone DFIG-DC System," *IEEE Transactions on Industrial Electronics*, vol. 64, no. 5, pp. 3502-3512, 2017.

[23] J. Arbi, M. J. B. Ghorbal, I. Slama-Belkhodja, and L. Charaabi, "Direct Virtual Torque Control for Doubly Fed Induction Generator Grid Connection," *IEEE Transactions on Industrial Electronics*, vol. 56, no. 10, pp. 4163-4173, 2009.

[24] S. El Daoudi, L. Lazrak, N. El Ouanjli, and M. Ait Lafkih, "Sensorless fuzzy direct torque control of induction motor with sliding mode speed controller," *Computers & Electrical Engineering*, vol. 96, p. 107490, 2021/12/01/ 2021.

[25] O. M. Kamel, A. A. Z. Diab, T. D. Do, and M. A. Mossa, "A Novel Hybrid Ant Colony-Particle Swarm Optimization Techniques Based Tuning STATCOM for Grid Code Compliance," *IEEE Access*, vol. 8, pp. 41566-41587, 2020.

[26] M. R. M. Hassan, M. A. Mossa, and G. M. Dousoky, "Evaluation of Electric Dynamic Performance of an Electric Vehicle System Using Different Control Techniques," *Electronics*, vol. 10, no. 21. doi: 10.3390/electronics10212586

[27] M. A. Mossa, O. M. Kamel, and S. Bolognani, "Explicit Predictive Voltage Control for an Induction Motor Drive," in *2019 21st International Middle East Power Systems Conference (MEPCON)*, 2019, pp. 258-264.

[28] C. Cheng and H. Nian, "Low-Complexity Model Predictive Stator Current Control of DFIG Under Harmonic Grid Voltages," *IEEE Transactions on Energy Conversion*, vol. 32, no. 3, pp. 1072-1080, 2017.

[29] L. L. Rodrigues, O. A. C. Vilcanqui, A. L. L. F. Murari, and A. J. S. Filho, "Predictive Power Control for DFIG: A FARE-Based Weighting Matrices Approach," *IEEE Journal of Emerging and Selected Topics in Power Electronics*, vol. 7, no. 2, pp. 967-975, 2019.

[30] M. A. Mossa and S. Bolognani, "Robust Predictive Current Control for a Sensorless IM Drive Based on Torque Angle Regulation," in *2019 IEEE Conference on Power Electronics and Renewable Energy (CPERE)*, 2019, pp. 302-308.

[31] M. A. Mossa, A. S. Al-Sumaiti, T. D. Do, and A. A. Z. Diab, "Cost-Effective Predictive Flux Control for a Sensorless Doubly Fed Induction Generator," *IEEE Access*, vol. 7, pp. 172606-172627, 2019.

[32] M. A. Mossa, H. Echeikh, and A. Iqbal, "Enhanced control technique for a sensor-less wind driven doubly fed induction generator for energy conversion purpose," *Energy Reports*, vol. 7, pp. 5815-5833, 2021/11/01/ 2021.

[33] S. G. Petkar and V. K. Thippiripati, "Enhanced Predictive Current Control of PMSM Drive With Virtual Voltage Space Vectors," *IEEE Journal of Emerging and Selected Topics in Industrial Electronics*, vol. 3, no. 3, pp. 834-844, 2022.

[34] M. Liu, K. W. Chan, J. Hu, W. Xu, and J. Rodriguez, "Model Predictive Direct Speed Control With Torque Oscillation Reduction for PMSM Drives," *IEEE Transactions on Industrial Informatics*, vol. 15, no. 9, pp. 4944-4956, 2019.

[35] M. E. Zarei, C. V. Nicolás, and J. R. Arribas, "Improved Predictive Direct Power Control of Doubly Fed Induction Generator During Unbalanced Grid Voltage Based on Four Vectors," *IEEE Journal of Emerging and Selected Topics in Power Electronics*, vol. 5, no. 2, pp. 695-707, 2017.

[36] P. Kou, D. Liang, J. Li, L. Gao, and Q. Ze, "Finite-Control-Set Model Predictive Control for DFIG Wind Turbines," *IEEE Transactions on Automation Science and Engineering*, vol. 15, no. 3, pp. 1004-1013, 2018.

[37] M. A. Mossa and S. Bolognani, "Predictive Power Control for a Linearized Doubly Fed Induction Generator Model," in *2019 21st International Middle East Power Systems Conference (MEPCON)*, 2019, pp. 250-257.

[38] G. F. Gontijo, T. C. Tricarico, B. W. França, L. F. d. Silva, E. L. v. Emmerik, and M. Aredes, "Robust Model Predictive Rotor Current Control of a DFIG Connected to a Distorted and Unbalanced Grid Driven by a Direct Matrix Converter," *IEEE Transactions on Sustainable Energy*, vol. 10, no. 3, pp. 1380-1392, 2019.